Formation of Mesopores in USY zeolites: a Case Revisited

Wolfgang Lutz, Rolf Kurzhals, Galina Kryukova, Dirk Enke, Manfred Weber, Detlef Heidemann

Zeitschrift für Anorganische und Allgemeine Chemie

Formation of Mesopores in USY zeolites: a Case Revisited

Journal:	*Zeitschrift für Anorganische und Allgemeine Chemie*
Manuscript ID:	zaac.201000025.R1
Wiley - Manuscript type:	Article
Date Submitted by the Author:	05-Feb-2010
Complete List of Authors:	Lutz, Wolfgang; BTU Cottbus, Luftchemie Kurzhals, Rolf; Süd-Chemie Zeolites GmbH Kryukova, Galina; Boreskov Institute of Ctalysis SBRAS Enke, Dirk; Martin-Luther-Universität Halle-Wittenberg Weber, Manfred; SCW Process Technology Development GmbH Heidemann, Detlef; Humboldt-Universität zu Berlin, Chemie
Keywords:	zeolite, dealumination, faujasite, mesopores

Formation of Mesopores in USY zeolites: a Case Revisited

W. Lutz[*1], R. Kurzhals[2], G. Kryukova[3], D. Enke[4], M. Weber[5], D. Heidemann[6]

[1] Berlin, Brandenburgische Technische Universität Cottbus

[2] Bitterfeld, Süd-Chemie Zeolites GmbH

[3] Novosibirsk, Boreskov Institute of Catalysis SBRAS, present address: Berlin, GNF e.V.

[4] Halle, Martin-Luther-Universität Halle-Wittenberg

[5] Berlin, Process Technology Development GmbH - SCW

[6] Berlin, Humboldt-Universität Berlin

Abstract

Steaming of NH_4Y zeolite at 723 K and 873 K is accompanied by the formation of extra-framework amorphous aluminosilicate and silica gel in addition to earlier observed extra-framework aluminium species. Their occurrence is directly associated with the formation of mesopores. Bulk (intracrystalline) mesopores occur inside the crystallite nuclei and surface (intercrystalline) mesopores are located nearby the crystallite surface. Corrosion of the zeolite framework results in a loss of crystallinity and, consequently, decreased catalytic activity of the USY catalysts synthesized. Analysis of the reasons of mesopore formation may help to reduce these disadvantages.

Keywords: zeolite, dealumination, faujasite, mesopores

* Wolfgang Lutz

Brandenburgische Technische Universität Cottbus, Volmerstr. 13, 12489 Berlin

Tel.: 0049 30 6392 4425

e-mail: lutz@ btu-lc.fta-berlin.de

1 Introduction

Much work has been done to characterize mesopores in ultra-stable Y zeolites (USY) [1-3] since the first reports on their dealumination by steam treatment which have been published almost four decades ago [4, 5]. However, debates over the origin of these mesopores are still continuing. It was generally assumed that this process results from the dealumination of the zeolite carcass followed by the appearance of extra framework aluminium species [6]. The secondary pore system was discussed to improve the molecular transport of educts and products in catalytic conversion processes.

Using texture analysis and 3D-TEM measurements Jansen et al. [7] were able to visualize in this material bulk mesopores surrounded by micropores in addition to cylindrical mesopores connected to the crystallite surface. Similar zeolite morphology was observed earlier by Lynch et al. who reported on a secondary pore system without direct connection to the exterior of the crystals in the steamed and, particularly, in acid leached USY samples [8]. The scheme given in Fig. 1 could elucidate the morphology of a USY particle with the two types of mesopores observed.

Kortunov et al. [9] have reported on molecular transport in the intracrystalline (bulk) mesopores of USY samples. These diffusion experiments have been performed using PFG NMR technique with n-octane and 1,3,5-triisopropylbenzene as probe molecules. Both molecules have critical molecular diameters smaller and larger than the inlet of the zeolite micropores. It was found that the mesopores inside the bulk do not affect diffusion of 1,3,5-triisopropylbenzene, therefore one could suggest that these mesopores are not connected with external crystallite surface and not able to contribute to the molecular transport.

Complicating the issue, the formation of siliceous extra-framework species in addition to the aluminium extra-framework admixture in USY has been recently reported [10]. Their occurrence was identified by ^{29}Si MAS NMR spectroscopic measurements as extra Si(4Al) and Si(0Al) signals with shapes different from those typical for the zeolite framework. These signals have been assigned to amorphous aluminosilicate and silica gel phases. Al- and Si-rich parts of the non-homogeneously crystallized Y zeolites of generally small particle size [11, 12] were suggested to contribute to the appearance of the extra siliceous species. It is highly

probable that these newly formed admixtures play important role in changing the total pore architecture of Y zeolites after the steaming.

This paper discusses, therefore, relationship between Si, Al extra-framework species and formation of mesopores in USY. A review on synthesis of NaY, dealumination procedure, appearance of extra-framework ions after the steaming process takes into consideration published works of the pioneers of zeolite chemistry. Along with experimental data reported in this paper, this overview could shed some light onto this well-known topic, being at the moment of renewed interest which relates to the chemistry of modern hierarchical porous zeolites. With this new knowledge on the reasons of mesopore formation in USY zeolites, one can hinder or at least minimize this effect during the synthesis of the initial NaY with a hope to obtain well crystalline zeolite Y frameworks.

2 Results and Discussion

Sample characterization

According to results of X-ray diffraction analysis (Fig. 2) the initial NaY sample is a pure FAU zeolite with the unit cell parameter a_0 = 2.4665 nm. Corresponding Si/Al ratio has been calculated using empirical relation (1) given by Rüscher et al. [13]

$$x = 5.348 a_0 - 12.898, \; a_0 \text{ in nm} \qquad (1)$$

(with Si/Al = (1-x)/x and x = Al molar fraction by use of the cell parameter a_0.).

With an average value of Si/Al = 2.6 the sample is suitable to be dealuminated without total collapse of the zeolite framework [12]. Owing to the removal of framework aluminium by steam treatment, the Si/Al ratio increases to 3.0 and 3.9 at 450°C and 600°C, respectively (Tab. 1). In this case 6% (USY, 450°C) and 16% (USY, 600°C) of an amorphous phase caused by the formation of extra-framework species [10] does appear. Whereas the particle size seems to remain the same as seen from SEM images given in Fig. 3, the diameter of the crystallites calculated from X-ray diffraction data decreases by 18% (450°C) and 19% (600°C), respectively (Tab.1).

The ^{27}Al MAS NMR spectrum of the initial NaY sample in Fig. 4 (A) shows a peak at 60 ppm usually assigned to aluminium atoms located in the tetrahedra inside the zeolite framework. The spectra of the USY samples (B, C) characterize extra-framework aluminium by signals lying between 0 and 3 ppm [14]. The broad shoulder centred at 30-35 ppm is assigned to pentahedrally coordinated Al species. This coordination state refers to the structural transition between tetrahedrally and octahedrally coordinated Al ions and gives a hint to the presence of specifically structured aluminium species [15].

Fig. 5 (A, I) shows the initial ^{29}Si MAS NNR spectrum of the parent NaY samples. After the deconvolution procedure (II), five signals typical of the NaY framework with Si(nAl) building units (n = 0-4) in the range of chemical shifts between –84 and –108 ppm become recognisable. Simulation of the signals was performed by use of a set of single lines with a Gaussian line shape (see Experimental section). The simulation procedure (III) did not reveal the presence of non-zeolitic siliceous admixtures in this sample.

A drastic change of the shape and intensity of NMR signals can be observed after the steaming of parent zeolite at 450°C (B, I) and 600°C (C, I). As evident from Fig. 5, peak positions are generally shifted to higher values. Intensity of peaks assigned to Si(4Al), Si(3Al), and Si(2Al) structure units decrease with simultaneous increase in intensity of signals related to Si(1Al) and Si(0Al) units due to dealumination effect. The line shape of the spectrum is changed in analogy to earlier results on a series of differently synthesized NaY samples [10], especially in the range of the low and high values of chemical shift. Furthermore, signal broadening and pronounced shoulders are observed in the region between –80 and –90 ppm and at about –112 ppm (B, II and C, II).

After deconvolution procedure, one can see additional signals of extra-framework species (B, III and C, III). These species are thought to be enriched in aluminium (Si(4Al)) and silicon (Si(0Al)), respectively. The signal height of Si(4Al) component, in opposite to the signal width with chemical shifts of -80 to –90 ppm (450°C) and –75 to –90 ppm (600°C), looks rather low but still visible after 4- and 8-fold multiplying of the signal intensity (dotted lines). It seems likely that the Al-rich material is strongly distorted.

By analogy with data given in ref. [10], both additional signals can be attributed to aluminosilicate (a) and silica gel (s) structures. High-alumina aluminosilicate can be detected directly using Molybdate measurements [16]. This aluminosilicate has numerous monomeric silicate units. But we were not able to find such short-chained silicates in our sample, probably they are encapsulated by the microporous USY matrix. But when we steamed high-alumina FAU zeolite of NH_4-LSX type at 450°C, we got more than 95% of monomeric silicate units with the help of Molybdate method. After steam treatment of same sample at 600°C, the Molybdate activity decreased significantly since the generated aluminosilicate have been transferred to Molybdate inactive species though we could not exclude formation of silicon and aluminium oxides too.

Contributions of silica gel superimpose strongly the ^{29}Si MAS NMR spectrum, particularly in the positions of Si(0Al) and Si(1Al) peaks [17]. Due to this fact, calculated Si/Al_{NMR} ratios

$$Si/Al = \Sigma_n I_n/(I_4+0.75I_3 + 0.5 I_2 + 0.25 I_1), \quad (2)$$

(*I_n = intensity of Q^4/nAl signals in ^{29}Si MAS NMR spectra, n = 0-4 [14])*

are generally higher than those calculated by use of the framework constant a_0. In our case, there are 4.2 (450°C) and 4.6 (600°C) against lower 3.0 and 3.9 values obtained from X-ray data ($Si/Al_{XRD,}$ see Tab. 1). This means, observed difference can speak in favour of the presence of silica gel admixture.

Partial phase transition observed by ^{29}Si MAS NMR spectroscopy is confirmed also by IR spectroscopic study. In Fig. 6 the asymmetrical TOT valence vibration (T=Si, Al) [18] changes from 1025 cm^{-1} (initial NaY) to 1047 cm^{-1} (450°C) and 1053 cm^{-1} (600°C) because of a strong superposition of signals of dealuminated zeolite Y matrix and newly formed silica gel. At the same time, double-ring vibration bands [19, 20] lying at 580 cm^{-1} (NaY), 586 cm^{-1} (450°C) and 592 cm^{-1} (600°C) become less resolved, particularly at the lower steaming temperature, due to the framework amorphization.

TEM observed some differences in the morphology of initial and treated zeolite crystallites, especially at the nanoscale level (Fig. 7). By rising steaming temperature, particle surface changes from the flat (NaY) into rough (USY, 450°, 600°C), even a thin outer surface layer appeared after steaming at 600°C which should be attributed to amorphous extra-framework material formed during sample treatment. Lynch et al. [8] have discussed this phenomenon as a capsulation of the solid crystalline part by an amorphous surface layer.

It was practically impossible to perform EDX analysis from the surface layers and bulk of the zeolites to compare Si and Al contents in different particle regions, since the signal coupling needs more than 5 min, a period sufficient for destroying the zeolite structure while irradiated with electron beam. However, TEM gives direct evidence that, though the composition is unknown, this surface layer or film is rather thin, being 2-3 nm in thickness. It is transparent but not smooth. Therefore, due to the critical size, the film could not be detected by XRD, with a further complication that this coverage looks like amorphous rather than crystalline.

From the results obtained one can see that neither XRD, NMR and IR analyses nor TEM give any evidence to the presence of any admixtures in the initial NaY zeolite. Therefore, formation of the siliceous extra-framework species in USY should result from a corrosion of the zeolite crystals themselves. Moreover, it seems probable that observed phase transition could be related to the generation of mesopores in the corroded USY framework.

Pore architecture

Nitrogen adsorption and mercury intrusion experiments show a significant change in pore structure due to the steaming procedure, in analogy to the results of Jansen [7] and Kortunov [9].

The nitrogen isotherm of the initial NaY sample (Fig. 8) shows mainly pure micropore adsorption. A high sorption level is reached already at the beginning of the nitrogen uptake and is finished at p/p_0 close to 0.1. The corresponding micropore surface and volume given in Tab. 2 have typical values of 989 m^2/g and 0.29 ml/g, respectively. The low contribution of mesopores to the total pore volume here results from the incomplete condensation of nitrogen in the inter-crystalline and inter-particle space of the NaY particles.

To make values of surface area and pore volume of NaY comparable to USY samples, they were extrapolated to theoretical *HNaY* stoichiometry because such modification cannot be prepared from NH_4NaY in practice without any dealumination. The stoichiometry of NaY differs in the elemental cell weight by 7.2% which should be taken into account if comparing the adsorption data (Tab. 2).

The micropore adsorption of USY steamed at 450°C (Fig. 8) is finished at $p/p_0 = 0.1$, too. At higher relative pressure of 0.83, a mesopore filling takes place and this process ends at 0.95. One can see a remarkable broad hysteresis which is typical for mesopores with restricted pore openings. The isotherm of the 600°C sample (Fig. 8) shows similar characteristics but the nitrogen volume consistent with hysteresis is higher, and a 2-step hysteresis is clearly visible. This behaviour is due to a significantly higher amount of mesopores which are formed inside the nuclei and nearby the crystallite surface.

With the increase of the mesopore surface from 10 m^2/g (450°C) to 24 m^2/g (600°C) the area of micropores decreases from 1060 m^2/g (*HNaY*) to 995 m^2/g (450°C) and 898 m^2/g (600°C). The mesopore volume of 0.021 ml/g and 0.064 ml/g increases in the same tendency whereas total and micropore volume decreases. Comparing to *HNaY,* one can see nearly two-fold increase of mesopore volume for USY (450°C) and its progressive growth for USY (600°C) due to higher effect of dealumination (Tab. 2).

According to mercury intrusion, the samples contain macropores of 100 to 10000 nm in diameter. These macropores characterize the space between the crystallites of the polycrystalline zeolite particles and their inter-particle space.

The macroporous structure of NaY with an average pore diameter of about 1700 nm appears to be similar to that of the USY (600°C) sample (Figs. 9). In contrast, the pore diameter of USY (450°C) is reduced to 1400 nm. It seems likely that at 450°C the space between the individual crystallites is filled out by a bigger quantity of extra-framework gel-type species.

Mesopores occur in a diameter range below 20 nm. They contribute to the total pore formation only to less than 1% (450°C) and 1.7 % (600°C). The corresponding pore volume amounts to <0.015 cm^3/g and 0.029 cm^3/g. Thus the pore volumes are smaller than those determined by nitrogen adsorption (right columns in Tabs 2 and 3). Due to the detection limit of mercury intrusion (minimum 3.8 nm pore opening), the Hg cannot penetrate all mesopores so that a part of them seems to be closed (bulk mesopores) and the other open (surface mesopores) as reported in refs. [7] and [9]. The volume of the open mesopores amounts to about the half of the total mesopore volume (Tabs. 2 and 3) so that the other half characterizes the closed mesopores surrounded by the microporous zeolite framework.

Formation of mesopores

Now we can get our experimental results and reference data by formulating the reason what is the driving force for the mesopore development during NaY steaming. Dealumination itself cannot be responsible for this effect because silicate ions migrate quickly into the newly created Al vacancies inside the USY framework [21, 22]. Some observations in the present work and in previous studies by means of ^{29}Si MAS NMR, XRD and IR spectroscopy [10] as well as energy-dispersive X-ray diffraction (EDXRD) measurements [23] give evidence to a partial amorphization of the zeolite Y crystals under action of steam.

Different behaviours in structural transformation of FAU crystals which depends on their chemical composition were found for series of X- and Y-type zeolites. Whereas X zeolites (Si/Al = 1.0-1.5) [12] and high-silica Y samples (Si/Al > 100) [24] were completely decomposed under hydrothermal stress, the structure of Y zeolites with medium composition (Si/Al = 2.3-2.7) has been changed only partially [10, 12]. In our case, the crystals of Y

zeolite with Si/Al ratio equal to 2.6 might be a mixture composed of X zeolite and high-silica Y phase. But the presence of such a mixture seems to be rather problematic due to observed corrosion effects, i.e. formation of mesopores inside the crystallites and on their surface [7, 9]. Therefore, specific behaviour of our sample upon thermal action of steam could be explained by a strong Si/Al gradient in its crystallites.

The semi-empirical approaches which describe the Si/Al ratio of FAU type zeolites by use of ^{29}Si MAS NMR [25] or X-ray data [26] did not take into account possible effect of such Si/Al gradient [27]. Due to fine size of the zeolite crystallites, it is difficult to get a direct proof of the gradient presence, e.g. using EDX analysis. According to our observation and data found here and in ref. [10], the crystallite size of all differently synthesised NaY samples amounts only to 85 - 225 nm. The crystallites form polycrystalline particles which diameter does not exceed 1000 nm (Tab. 1). The Si/Al gradient equalizes thus over the volume of the separate NaY particle. But to explain the phenomenon of inhomogeneous structural state of NaY zeolite, we may suggest the following scheme based on the NaY crystallization mechanism.

The synthesis of NaY begins usually with a fast soluble source for aluminate and a slowly soluble source for silicate molecules given in excess [28-30]. As a result of mixing them, a compact SiO_2 gel including the complete amount of dissolved aluminate ions precipitates at first. Owing to successive dissolution of the SiO_2 gel, short-chained silicate ions are formed. Of about 10% of the total amount of SiO_2 involved was found to be assembled in the short-chained aluminosilicate molecules with a ratio of Si/Al close to one [31]. They are relatively stable in the mother liquor at room temperature [32, 33]. However, at the elevated synthetic temperature (e.g. 90°C) these molecules re-arrange and form seeds of the X-type zeolite that initiate a crystal growth. Frequently, X-type seeds are added purposely into synthesis batch in order to direct and accelerate the growth of zeolite Y crystal [30, 34-35].

With increasing synthesis time, such growing crystals change their Si/Al distribution at the surface with a ratio greatly exceeding one due to the uptake of the dissolved silicate ions being meanwhile in excess [36]. Thereby, it is a common observation that the batch in the final state still contains big excess of non-reacted silicate. Because of the non-adequate Al-consumption at the beginning of crystallization, the concentration of the aluminate ions gets finally too low to promote further a formation of sodalite cages as building units of the FAU

structure [28-30]. This fact explains why NaY samples with Si/Al ratios lying above 2.2 have the limited crystal size [12].

The Al-rich nucleus of zeolite Y is decomposed under action of water molecules by "acid" hydrolysis of the framework [10]. The formed silicate and aluminate ions react to produce aluminosilicate below 450°C [37] and additionally Si and Al oxides at 600°C [16].

But formation of aluminosilicate requires sodium ions which are present mainly in the nucleus of NaY crystallite. Indeed, our samples contain residual sodium ions in a concentration as high as 20%. But these extra ions seem to be distributed over the whole crystallite volume of the actual Y sample as a result of homogeneous NH_4^+/Na^+ ion exchange at the first step of the steaming procedure so that the formation of aluminosilicate is reduced. However, the strong signal of pentahedrally coordinated aluminium in the ^{27}Al MAS NMR spectrum in Fig. 4 (B) gives a hint to the decomposition of the nuclei in the USY crystals. The shape of Si(nAl) signals in the ^{29}Si MAS NMR spectra provides further evidence for the possible existence of Si/Al gradient. While similar signals obtained from zeolite NaX and, particularly zeolite NaA are sharp because of their homogeneous environments, the Si(nAl) spectral peak in NaY noticeably broadens that may indicate to Si/Al gradient in zeolite particles [14].

At the same time, the Si-rich surface of Y crystals decomposes according to the "alkaline" mechanism [10] that leads to the formation of silica gel. The appearance of new hydroxyl groups [38] indicates particularly this process. TEM micrographs given in Fig. 7 show the result of this process as a significantly changed surface morphology with a thin extra surface layer. The observed shell is called "silica-alumina" [39] because it involves also the octahedrally coordinated extra-framework Al species which presence was confirmed by XPS measurements [40]. The corrosion of the crystallite surface [1] proceeds simultaneously with the shrinking of the crystallite diameter up to 20% due to the removal of framework aluminium (Tab. 1). Obviously, XRD particle sizes given in Table 1 could not be considered as absolute values calculated with Scherrer equation since the determination error in the case of well crystalline samples is usually big. But using our XRD diffractometer and software package along with internal Si standard we were able to register the broadening of the characteristic XRD peaks in USY comparing to that of the initial zeolite. Therefore, rather than provide the absolute crystallite values, we show here the tendency in the change of crystallite diameter in the initial and steamed samples.

Present evidence allows us to propose a generalised structural model of the micropores formation based on the concept of the siliceous extra-framework species in the steamed USY zeolites. During steaming parts of the zeolite Y are decomposed. This process is accompanied by the formation of silica gel on the crystal surface and amorphous aluminosilicate inside the zeolite framework. Both phases possess higher density compared to that of the zeolite framework which leads inevitably to the generation of mesopores inside the zeolite bulk, particularly in the nuclei of the USY crystallites [7, 9]. Important to this concept is a suggestion that initial NaY zeolite crystallites have a systematic Si/Al gradient with a high portion of silicon at the crystal surface and increased content of aluminium in the centre of crystallites. This gradient, being structural feature of the Y zeolite, reflects on specific synthesis mechanism of this zeolite type.

3 Conclusions

The crystallites of initial NaY zeolite seem to have a systematic Si/Al gradient. Because they are generally small in size [41] and form polycrystalline particles it is difficult to get the solid experimental evidence for the detection of this phenomenon. But it can be characterized indirectly by evaluation of the hydrothermal stability of the framework and analysis of decomposition products of the transformations of NH_4NaY (ion exchange) into USY modification (steam treatment). Steaming results in formation of two types of mesopores: closed bulk (intracrystalline) mesopores surrounded by the micropores of the zeolite framework and open surface (intercrystalline) mesopores at the crystallites surface. Former are generated by decomposition of the Al-rich nuclei while latter appears as a result of the partial destruction of the Si-rich surface. The open surface mesopores are in direct contact to the internal macropores of the polycrystalline zeolite particles. Because of partial decomposition of the resulting USY zeolite, further extra-framework siliceous species are formed, in addition to the well-known pentahedrally and octahedrally coordinated extra-framework aluminium. There are silica gel at the crystallite surface and aluminosilicate inside the framework. Thus, the generation of mesopores is directly associated with the formation of the siliceous extra-framework species. Their occurrence leads to a loss of crystallinity and decrease of the catalytic active sites of Brønsted type. More homogeneous Si and Al distributions in the parent NaY zeolites which could be possible to achieve via new synthesis pathways can reduce the crystal corrosion.

4 Experimental section

Commercial NaY zeolite of the GRACE Division was investigated. Ammonium form of the samples with a particle size distribution of 0.4 - 1.0 μm obtained by a three-fold ion exchange in 0.1 M aqueous solution of NH_4NO_3 at room temperature for 1 hour in each step by use of a liquid/solid mass ratio of 100 was used. The obtained NH_4NaY zeolite was washed with deionised water and dried at 120°C for 1 hour. The ion exchange was limited in analogy to earlier observation [42] to 79%.

The sample treatment was performed in steam under pressure of 1bar at 450°C or 600°C for 7 hours. The heating rate of the process was equal to 10°C per minute. The sample was contacted with steam after reaching the choosing temperature.

The obtained USY zeolite was characterized in the hydrated state by X-ray diffraction, ^{29}Si MAS NMR measurement, IR spectroscopy, SEM and TEM, nitrogen adsorption, mercury porosity and Molybdate measurements.

The XRD data were recorded on a Philips PW 1800 powder diffractometer equipped with a graphite monochromator and Cu Kα radiation at 40 kV and 40 mA. Measurements were performed in the 2θ range between 5 ° and 85 ° with a step of 0.03 ° and a coupling time of 1 s count per step. The powder patterns were measured with SuperQ software from Philips Analytical B. V., Almelo. XRD patterns were evaluated by using of the Profit-software (Philips Electronics N. V.) as well as a self-developed program for calculation of lattice constants, relative crystallinity and crystallite sizes. The crystallite size calculations were performed using Scherrer equation with internal standard of well crystalline Si powder.

The solid-state NMR spectra were recorded at room temperature on a Bruker Avance 400 spectrometer, operating at frequencies of 104.3 MHz for ^{27}Al and 79.5 MHz for ^{29}Si. A 4 mm double tuned (^{1}H-X) MAS probe (Bruker Biospin) was used to perform MAS NMR measurements at spinning rates of 14 kHz in the ^{27}Al MAS experiments and 12 kHz in the ^{29}Si MAS experiments, respectively. The ^{27}Al MAS spectra were obtained using single pulse excitation with pulse durations of 1 μs (π/12 pulses). Up to 1024 scans were recorded with a recycle delay of 1s. The ^{29}Si MAS spectra were obtained using single pulse excitation consisting of 4 μs pulses (π/2 pulses) and recycle delays of 120 s to exclude saturation effects.

Up to 700 FIDs were accumulated to obtain reliable signal-to-noise ratio. The ^{27}Al and ^{29}Si spectra were externally referenced to 1 M aqueous $AlCl_3$ solution and to liquid Me_4Si at 0 ppm, respectively. The quantitative line shape analysis of the ^{29}Si MAS NMR spectra has been performed by use of the dmfit software package [43]. Every resolved component of the experimental NMR spectra was described by only one single line with a pure Gaussian line shape. The position (chemical shift), the line width and the altitude (height) of the corresponding lines were optimized by a least square fit using this program. The relative intensities of the components of every simulated spectrum were obtained by integrating over the component line compared to the total integral over all component lines of the simulated spectrum.

IR absorption spectra were taken on a Shimadzu FTIR 8400S spectrometer with a resolution of ± 1 cm^{-1} by use of 30 scans. For analysis, 0.5 mg of the sample was pressed with 400 mg KBr into a pellet while spectra were registered in the IR range from 400 to 4000 cm^{-1}.

SEM analysis was conducted with JSM-6460 LV JEOL scanning electron microscope at the resolution power of 3 nm in low vacuum (10 Pa), without sputtering the conducting layer on the surface of zeolite particles.

TEM analysis was performed with JEM-2010 JEOL transmission electron microscope at 100 kV accelerating potential and 1 nm resolution limit. After ultrasonic treatment of the sample in alcohol, the drop of this suspension was placed onto a holey-carbon copper grid for TEM observation. To prevent possible collapse of the zeolite structure which often occurs during observation of this material at the electron microscope column, we used special low dose regime with a decreased intensity of the incident electron beam. This enabled us to focus the image and to take a micrograph in a short time (less than 2 min), without any observable changes in the zeolite structure or the hole drilling.

Nitrogen sorption measurements were performed by use of a Sorptomatic 1990 apparatus by ThermoFinnigan. All samples were degassed at 623 K before measurement for at least 24 hours at 10^{-5} mbar. Adsorption and desorption isotherms were measured over a range of relative pressures (p/p_0) from 0 to 1.0. The surface area of the micropores $O_{S,\ micro}$ and the micropore volume $V_{P,\ micro}$ were determined according to Dubinin-Radushkevich-Kaganer [44]. The total pore volume V_P was estimated from the amount of gas adsorbed at the relative

pressure $p/p_0 = 0.996$ assuming that pores were filled subsequently with condensed adsorptive in the normal liquid state. The t-plot method [45] was used to determine the surface area of the mesopores $O_{S,\,meso}$. Finally, the mesopore volume $V_{P,\,meso}$ was calculated according to

$$V_{P,\,meso} = V_P - V_{P,\,micro}. \quad (3)$$

The mercury intrusion measurements were carried out on a Pascal 440 apparatus by ThermoFinnigan. The cumulative pore volume at a given pressure represents the total volume of mercury taken up by the sample at that pressure. A contact angle of 141.3° for Hg and a cylindrical pore model were used to interpret the results using the Washburn equation [46].

For Molybdate measurements 5 mg of the samples were dissolved in 100 ml of a 10^{-2} M hydrochloric acid at 273 K in which the -Si-O-Al- bonds are hydrolysed immediately whereas the -Si-O-Si- polymer building units are stable. By the following treatment at 298 K the silicate units are decomposed in the presence of 2 ml of a 10% solution of molybdic acid. The molybdic acid only reacts with monomeric silicate ions giving rise to the yellow β-dodecamolybdato silicic acid complex. Its formation depends on the degradation velocity of the polymeric silicate units. The process is followed spectroscopically at a wavelength of 400 nm with a Shimadzu UV-1601 spectrometer. The slope of the resulting curves is a direct function of the degree of condensation of the formed silicate units. It may be noted that the degree of condensation of the silicate units in aluminosilicates generally decreases with increasing substitution of silicon by aluminium atoms.

References

[1] U. Lohse, H. Stach, H. Thamm, W. Schirmer, A. A. Isikrikjan, N. I. Regent, M. M. Dubinin, Z. anorg. allg. Chem. **1980**, *460*, 179.

[2] G. Weber, M.H. Simonot-Grange, ZEOLITES **1994**, *14*, 433.

[3] C. S. Triantafillidis, A. G. Vlessides, N. P. Evmiridis, Ind. Eng. Chem. Res. **2000**, *39*, 307.

[4] C.W. McDaniel, P. K. Maher, P.K., Molecular Sieves, Soc. Chem. Ind., London **1968**, p. 186.

[5] P. K. Maher, F. D. Hunter, J. Scherzer, Advanc. Chem. Ser. **1971**, *101*, 266.

[6] G. T. Kerr, J. Catal. **1969**, *15*, 200.

[7] A. H. Jansen, A. J. Koster, K. P. de Jong, Angew. Chem. Int. Edt. **2001**, *40*, 1102.

[8] J. Lynch, F. Raatz, P. Dufrense, ZEOLITES **1987**, *7*, 333.

[9] P. Kortunov, S. Vasenkov, J. Kärger, R. Valiullin, P. Gottschalk, M. Fé Elí, M. Perez, M. Stöcker, B. Drescher, G. McElhiney, C. Berger, R. Gläser, J. Weitkamp, J. Am. Chem. Soc. **2005**, *127/37*, 13055.

[10] W. Lutz, H. Toufar, D. Heidemann, N. Salman, C.H. Rüscher, T.M. Gesing, J.-Chr. Buhl, R. Bertram, Microp. Mesop. Mater. **2007**, *104*, 171.

[11] C. Berger, R. Gläser, R.A. Rakoczy, J. Weitkamp, Micropor. Mesopor. Mater. **2005**, *83*, 333.

[12] C.H. Rüscher, N. Salman, J.-Chr. Buhl, W. Lutz, Microp. Mesop. Mater. **2006**, *92*, 309.

[13] C.H. Rüscher, J.-Chr. Buhl, W. Lutz, in A. Galarneau, F. Di Renzo, F. Fajula, and J. Vedrine (Eds.), Stud. Surf. Sci. Cat., Vol. 135, Elsevier, Amsterdam, **2001**, 13-P15, p. 1.

[14] G. Engelhardt, D. Michel, in: High Resolution Solid State NMR of Silicates and Zeolites, Wiley & Sons, New York, **1987**.

[15] K.U. Gore, A. Abraham, S.G. Hedge, R. Kumar, J.-P. Amoureux, S. Ganapathy, J. Phys. Chem. B, **2002**, *106*, 6115.

[16] R. K. Iler, The chemistry of Silica, Wiley & Sons, New York, **1979**.

[17] W. Lutz, D. Heidemann, C. Hübert, W. Wieker, Z. Anorg. Allg. Chemie, **2001**, *627* 2559.

[18] H. Fichtner-Schmittler, U. Lohse, H. Miessner, H.-E. Maneck, Z. phys. Chem. – Leipzig, **1990**, *271*, 69.

[19] E. M. Flanigen, H. Khatami, H. A. Szymanski, Adv. Chem. Ser. **1971**, *101*, 201.

[20] E.M. Flanigan, in: J.A. Rabo (ed.), Zeolite Chemistry and Catalysis, ACS Monographs, **1976**, *171*, 81.

[21] A.T. Steel, E. Dooryhee, ZEOLITES, **1993**, *13*, 336.

[22] U. Lohse, M. Mildebrath, Z. anorg. allg. Chem. **1981**, *476*, 126.

[23] G.J. Ray, B.L. Meyers, C.L. Marshall, ZEOLITES, **1987**, *7*, 307.

[24] K. Ehrhardt, M. Suckow, W. Lutz, in: H. K. Beyer, H. G. Karge, I. Kirici and J. B. Nagy (Eds.), Catalysis by Microporous Materials, Stud. Surf. Sci. Catal., Vol. 94, Elsevier, Amsterdam, **1995**, p. 179.

[25] D. Ding, B. Li, P. Sun, Q. Jin, J. Wang, ZEOLITES **1995**, *15*, 569.

[26] V. Jorik, ZEOLITES **1993**, *13*, 187.

[27] A. Corma, F.V. Melo, D.J. Rawlence, Zeolites, **1990**, *10*, 690.

[28] R. Barrer, *Hydrothermal Chemistry of Zeolites*, Academic Press, London, **1982**.

[29] D.W. Breck, *Zeolite Molecular Sieves*, John Wiley & Sons, London, **1974**.

[30] S. P. Zhdanov, S. S. Khvoshchev, N. N. Feoktistova, *Synthetic Zeolites*, Gordon & Breach Science Publishers, New York, **1990**.

[31] B. Fahlke, W. Wieker, H. Fürtig, W. Roscher, R. Seidel, Z. anorg. allg. Chem. **1978**, *439*, 95.

[32] S. P. Zhdanov, E. N. Egorova, *Chimija Zeolitov*, Isd. Nauka, Leningrad, **1968**, p. 80.

[33] T. Antonić, A. Čižmek, C. Kosanović, B. Subotić, J. Chem. Soc. Faraday Trans. **1993**, *89*, 1817 (Part I) and T. Antonić, A. Čižmek, B. Subotić, J. Chem. Soc. Faraday Trans. **1994**, *90*, 1973 (Part II).

[34] G. Clet, J. C. Jansen, Chem. Mater. **1999**, *11*, 1696.

[35] B. Sarkar, K. Arya, G. Ravichandran, M. P. Kuvetta, S. P. Choudhury, V. Krishnan, S. K. Ray, J. Christopher, S. Makhija, USP 20,080,182,744.

[36] H. Kasirek, H. Lechert, J. Phys. Chem. **1975**, *79*, 1589.

[37] D. P. Siantar, W. S. Millmann, J. J. Fripiat, ZEOLITES **1995**, *15*, 556.

[38] U. Lohse, E. Löffler, M. Hunger, J. Stöckner, V. Patzelová, ZEOLITES **1987**, *7*, 11.

[39] M. Stockenhuber, J. A. Lercher, Microp. Mat. **1995**, *3*, 457.

[40] E. Merlen, J. Lynch, M. Bisiaux, F. Raatz, Surf. Interf. Analysis **1990**, *16*, 364.

[41] C. Berger, R. Gläser, R.A. Rakoczy, J. Weitkamp, Micropor. Mesopor. Mater. 83 (2005) 333.

[42] N. Salman, C. H. Rüscher, J.-Chr. Buhl, W. Lutz, H. Toufar, M. Stöcker, Microp. Mesop. Mat. **2006**, *90*, 339.

[43] D. Massiot, F. Fayon, I. King, S. Le Calvé, B. Alonso, J.O. Durand, B. Bujoli, Z. Gan, G. Hoatson, Mag. Reson. Chem., **2002**, *40*, 70.

[44] M.M. Dubinin, L.V. Radushkevich, Proc. Acad. Sci. **1947**, *55*, 331.

[45] B.C. Lippens, B.G. Linsen, J.H. de Boer, J. Catalysis **1964**, *3*, 32.

[46] E.W. Washburn, Proc. Nat. Acad. Sci. USA, **1921**, *115*, 7.

Captions to the Tables

Tab. 1 Characteristic data of the initial NaY and the steamed USY zeolites

Tab. 2 Pore volume and surface area of the initial NaY and the steamed USY zeolites determined by nitrogen sorption uptake measurements

Tab. 3 Pore characteristic of the initial NaY and the steamed USY zeolites determined by mercury intrusion measurements

Tab. 1 Characteristic data of the initial NaY and the steamed USY zeolites

Zeolite	a_o nm	Si/Al ratio [1)] XRD	NMR	SEM size of primary particles, nm	XRD size of crystallites, nm	degree of crystallinity, %
NaY	2.465	2.6	2.6	400 – 1000	225	100
USY, 450°C	2.458	3.0	4.2	400 – 1000	184	94
USY, 600°C	2.441	3.9	4.6	400 – 1000	182	84

[1)] values are determined by use of the lattice constant a_0 and ^{29}Si MAS NMR signal intensities according to eqs. (1) and (2), respectively

Tab. 2 Pore volume and surface area of the initial NaY and the steamed USY zeolites determined by nitrogen sorption uptake

Sample	micropore surface m^2/g	mesopore surface m^2/g	total volume ml/g	micropore volume ml/g	mesopore[2)] volume ml/g	mesopore[3)] volume Δ ml/g
NaY	989	-	0.31	0.29	0.007	-
HNaY [1)]	*1060*	-	*0.32*	*0.31*	*0.007*	*0*
USY, 450°C	995	10	0.31	0.28	0.021	0.014
USY, 600°C	898	24	0.31	0.24	0.064	0.057

[1)] NaY values extrapolated to theoretical *HNaY* (20% sodium ions) modification according to the mass difference of 7,2%

[2)] difference of total to micropore volume

[3)] difference of USY and *HNaY* pore volume

Tab. 3 Pore characteristics of the initial NaY and the steamed USY zeolites determined by mercury porosimetry

zeolite	average pore diameter nm	total porosity %	bulk density g/cm^3	total volume ml/g	total surface m^2/g	mesopore volume ml/g
NaY	1680	43	0.294	1.45	5.59	0
USY, 450°C	1397	63	0.412	1.53	10.623	< 0.015
USY, 600°C	1682	68	0.395	1.73	21.259	0.029

Caption to the Figures

Fig. 1 Morphology of a USY zeolite particle

Fig. 2 X-ray diffraction pattern of the initial NaY (A) and the USY zeolites steamed at 450°C (B) and 600°C (C)

Fig. 3 SEM micrographs of the initial NaY (A) and the USY zeolites steamed at 450°C (B) and 600°C (C)

Fig. 4 ^{27}Al MAS NMR spectra of the initial NaY (A) and the USY zeolites steamed at 450°C (B) and 600°C (C)

Fig. 5 ^{29}Si MAS NMR spectra of the initial NaY (A) and the USY zeolites steamed at 450°C (B) and 600°C (C)
(I measured spectra, II deconvoluted spectra, III difference of I to II, extra-framework aluminosilicate (a) and silica gel (s))

Fig. 6 IR spectra of the initial NaY (A) and the USY zeolites steamed at 450°C (B) and 600°C (C)

Fig. 7 TEM micrographs of the initial NaY (A) and the USY zeolites steamed at 450°C (B) and 600°C (C)

Fig. 8 Nitrogen sorption uptake of the initial NaY (A) and the USY zeolites steamed at 450°C (B) and 600°C (C)

Fig. 9 Mercury uptake of the initial NaY (A) and the USY zeolites steamed at 450°C (B) and 600°C (C)

Fig. 1 Morphology of a USY zeolite particle

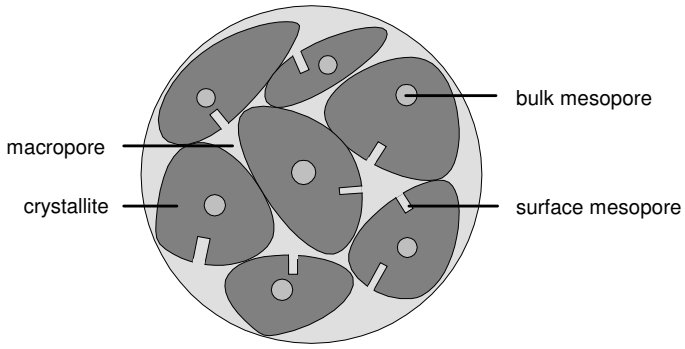

Fig. 2 X-ray diffraction pattern of the initial NaY (A) and the USY zeolites steamed at 450°C (B) and 600°C (C)

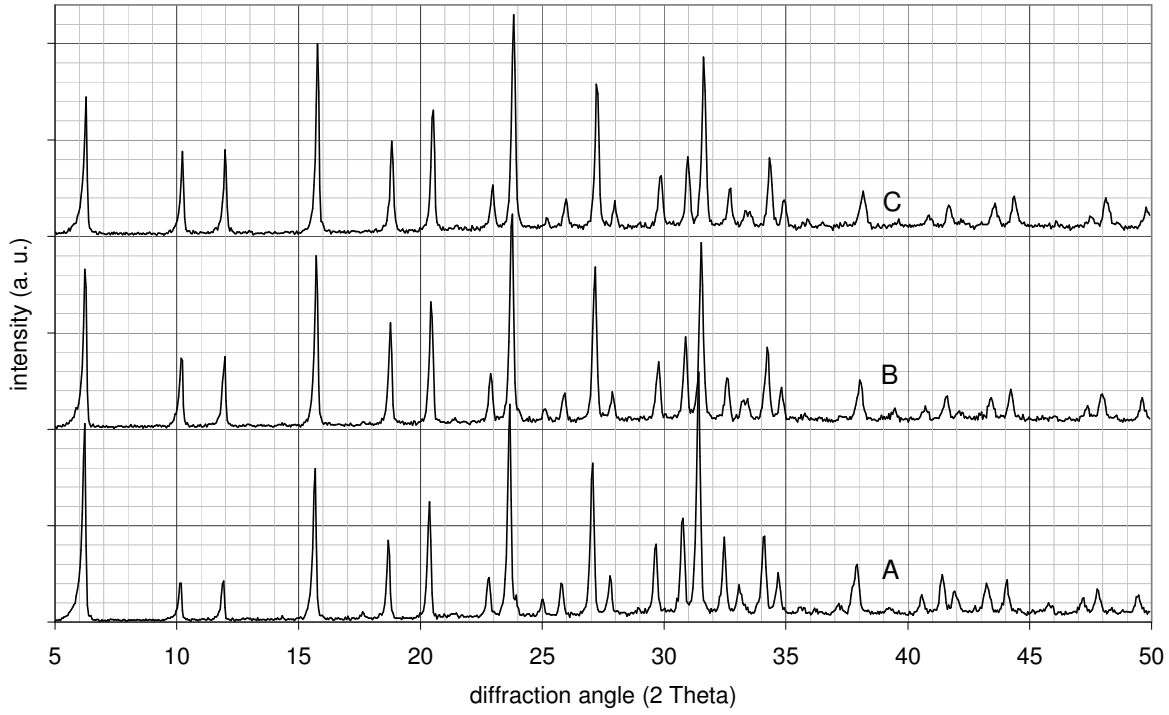

Fig. 3 SEM micrographs of the initial NaY (A) and the USY zeolites steamed at 450°C (B) and 600°C (C)

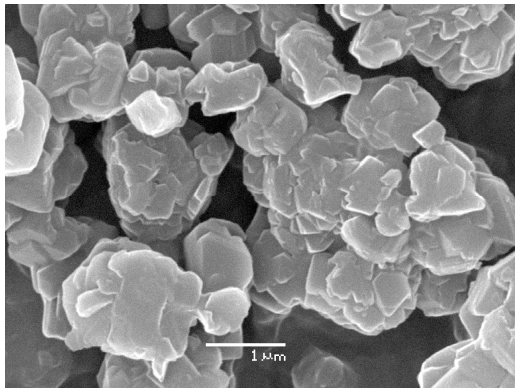

A

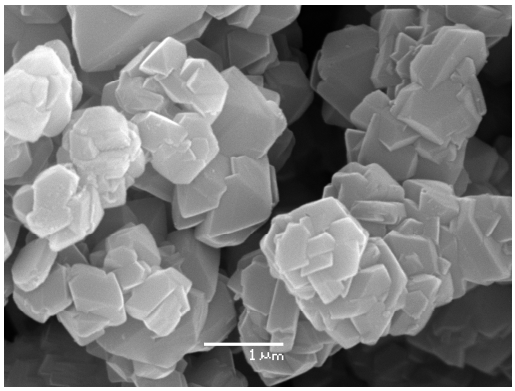

B

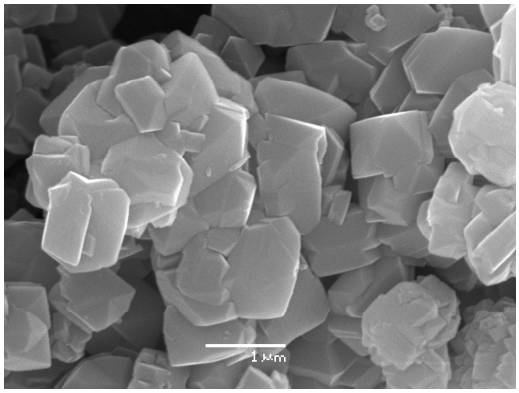

C

Fig. 4 ^{27}Al MAS NMR spectra of the initial NaY (A) and the USY zeolites steamed at 450°C (B) and 600°C (C)

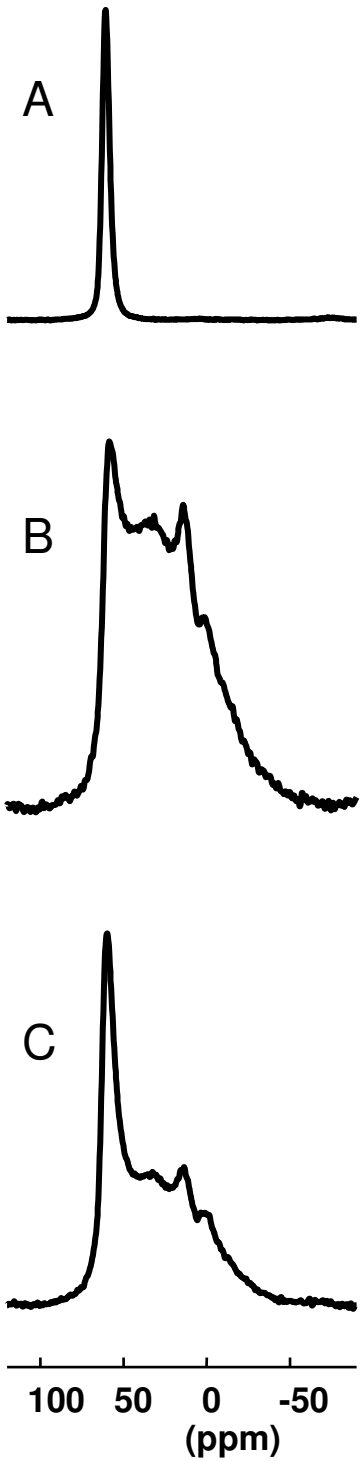

Fig. 5 ^{29}Si MAS NMR spectra of the initial NaY (A) and the USY zeolites steamed at 450°C (B) and 600°C (C)

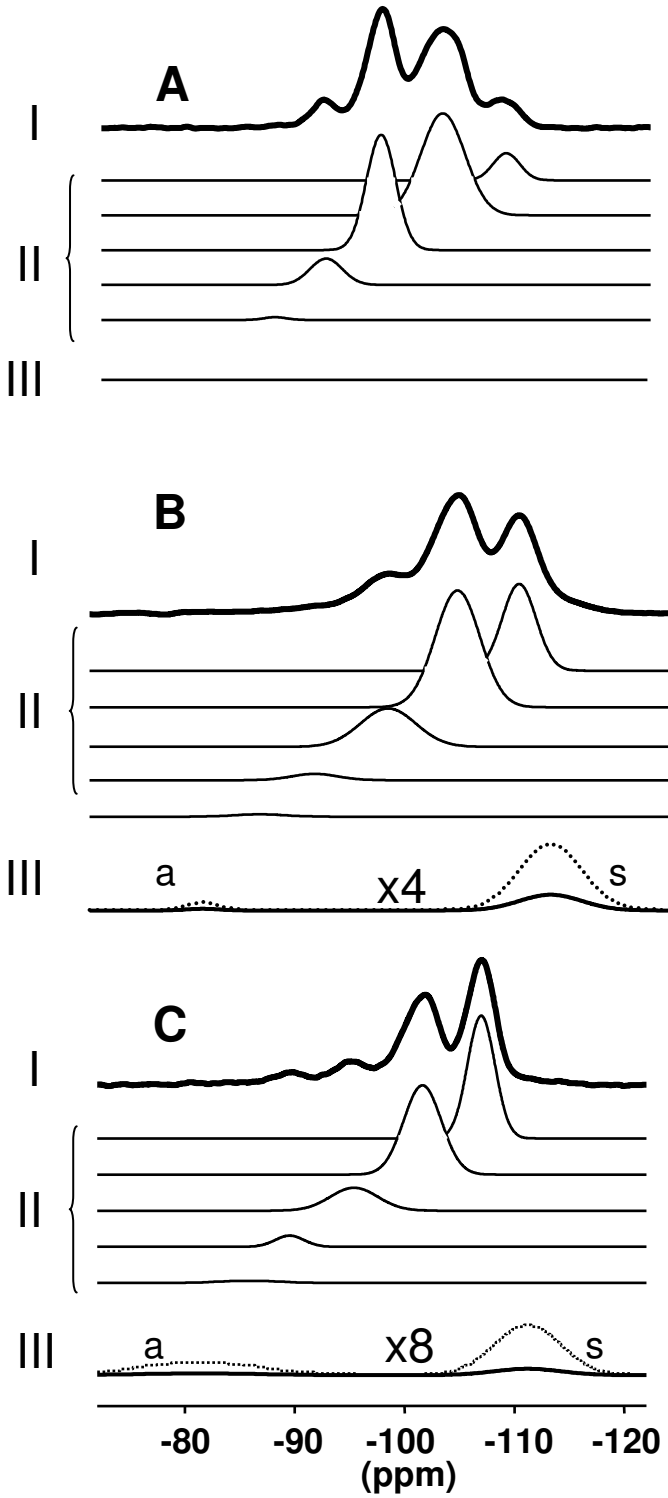

Fig. 6 IR spectra of the initial NaY (A) and the USY zeolites steamed at 450°C (B) and 600°C (C)

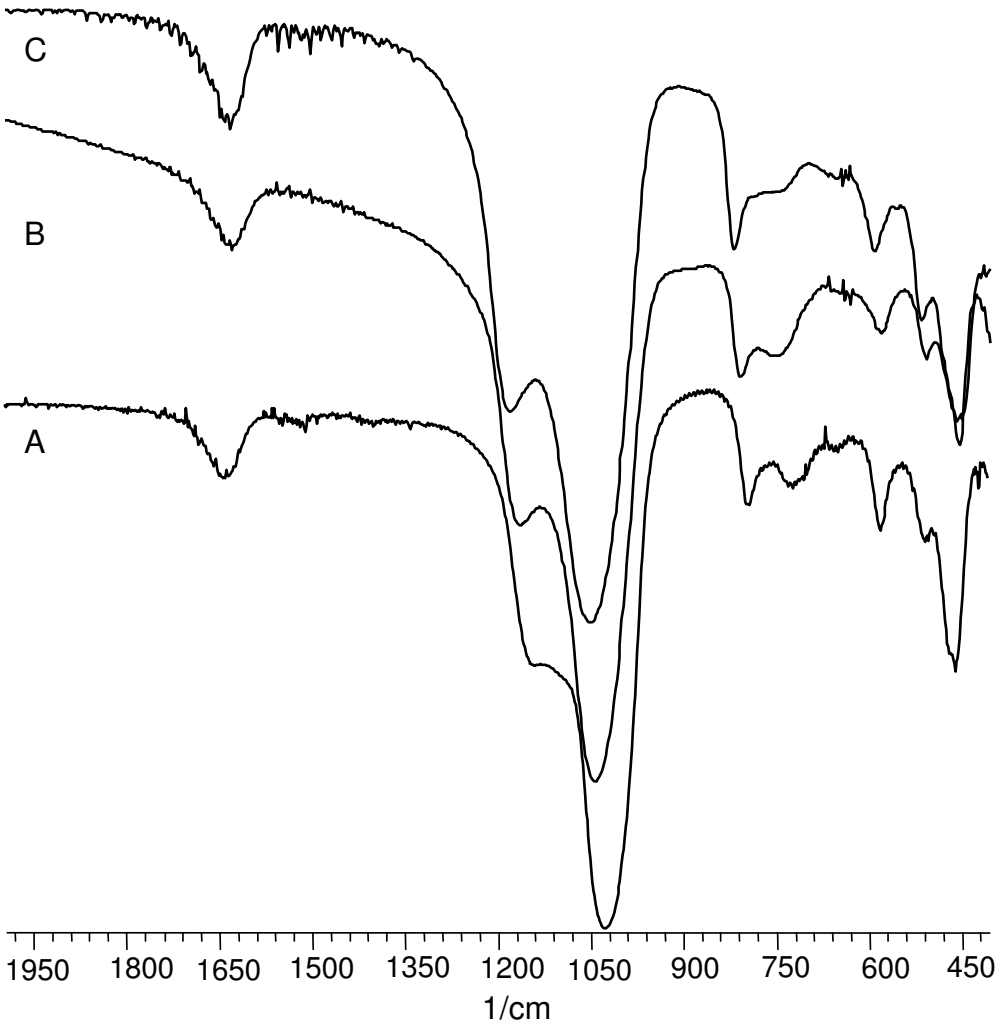

Fig. 7 TEM micrographs of the initial NaY (A) and the USY zeolites steamed at 450°C (B) and 600°C (C)

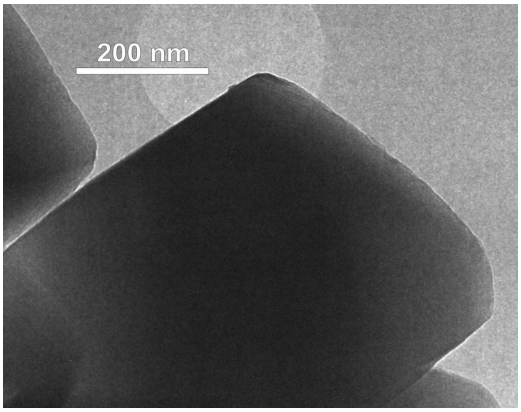

A

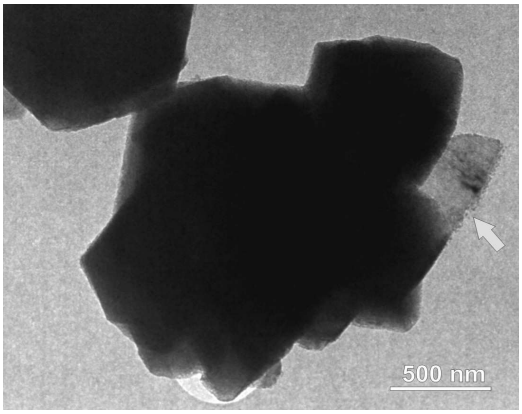

B

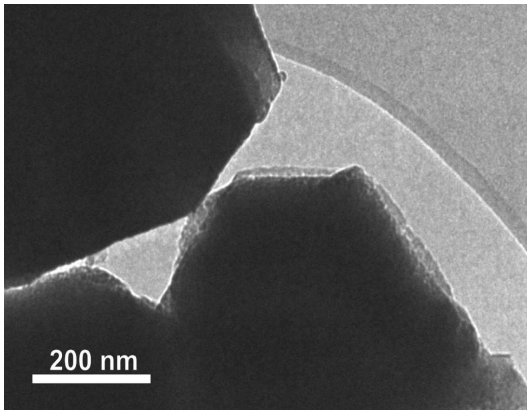

C

Fig. 8 Nitrogen sorption uptake of the initial NaY (A) and the USY zeolites steamed at 450°C (B) and 600°C (C)

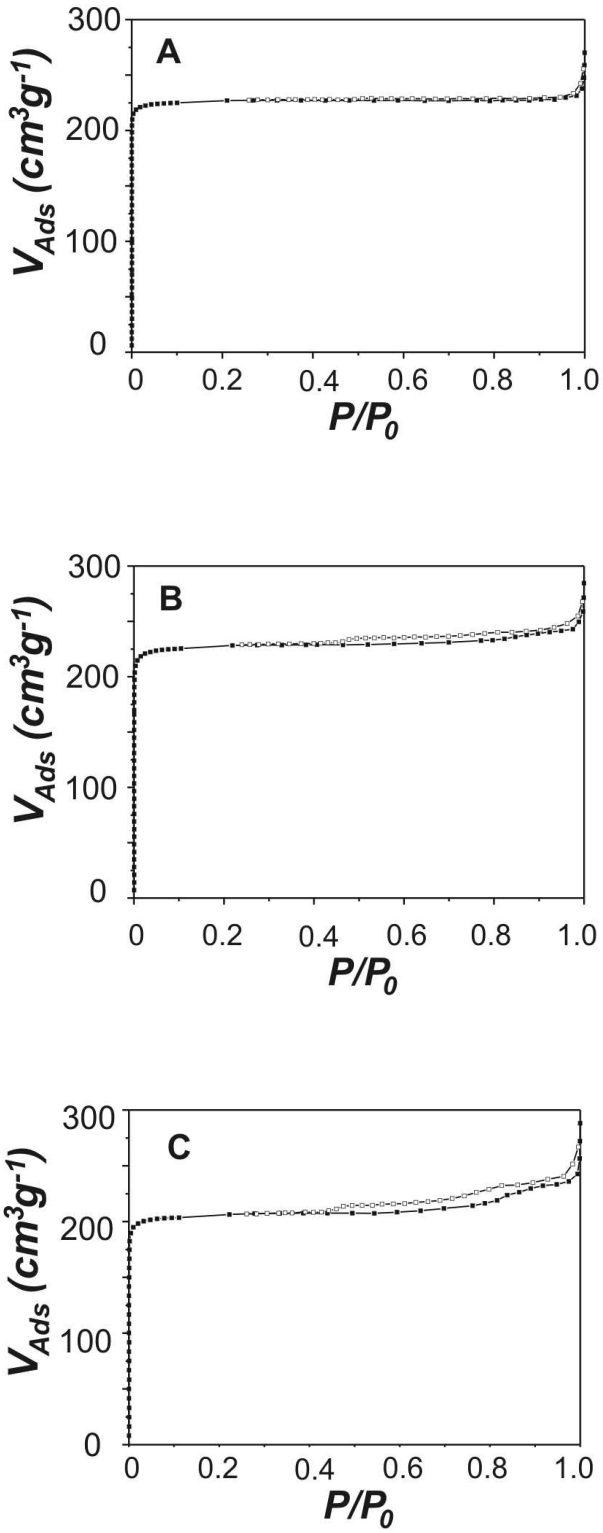

Fig. 9 Mercury uptake of the initial NaY (A) and the USY zeolites steamed at 450°C (B) and 600°C (C)